Rare-earth titanate melt structure and glass formation

O.L.G. Alderman[a,*], C.J. Benmore[b], A. Tamalonis[a], R. Weber[a,b]

a. Materials Development, Inc., Arlington Heights, IL 60004, USA

b. X-Ray Science Division, Advanced Photon Source, Argonne National Laboratory, Argonne, IL 60439, USA

*Corresponding author o.alderman@gmail.com

Abstract

The structure of rare-earth titanate melts and glasses of composition $17RE_2O_3.83TiO_2$ have been investigated *in-situ* by aerodynamic levitation with laser heating. Ti K-edge x-ray absorption near-edge structure (XANES) spectroscopy reveals an effect of RE cation size on mean Ti–O coordination numbers (n_{TiO}), which increase from ~4.8(2) in glass-forming La titanate to ~5.1(2) in non-glass-forming Sc titanate liquids. We suggest that the associated increase in OTi_3 triclusters in melts bearing smaller RE cations tends to inhibit glass formation. Both XANES and high-energy x-ray diffraction indicate increases in n_{TiO} as the liquids supercool and vitrify. Results are discussed in the context of alkali and alkaline-earth titanate glasses, extending the observed dependence of n_{TiO} on structural basicity (modifier content divided by potential) to trivalent modifiers and the molten state. We suggest that the most stable titanate glasses form close to compositions where, on average, two oxygen anions bond to each titanium, allowing a continuous, disordered Ti–O network of bridging oxygen (OTi_2), or with equal numbers of OTi_3 triclusters and OTi_1 non-bridging oxygen in charge-balance. We report on new glasses formed from praseodymium, europium and gadolinium titanate melts, the latter being the smallest rare-earth for which binary titanate glasses have been obtained.

1. Introduction

Glass formation from rare-earth titanate liquids is possible over narrow compositional ranges, where TiO_2 content typically exceeds 80 mol%, or 66.7 cation % titanium (Table 1).[1, 2] Such glasses have exceptionally high refractive indices, in the region of $n_d \simeq 2.3$,[3, 4, 5, 6] which approaches that of amorphous TiO_2[7, 8] or crystalline diamond.[9] Combined with low dispersion (Abbe numbers of $v_d \simeq 20$),[4] rare-earth titanate glasses are well suited for compact optical and photonic applications, including as microspheres for retroreflective coatings[10] and lenses for super-resolution optical microscopy beyond the diffraction limit.[11] Furthermore, RE_2O_3–TiO_2 glasses have high thermal and chemical stabilities and offer high solubility of optically active rare-earth dopants. These properties have led to the demonstration of bright-white

upconversion luminescence from lanthanum-ytterbium titanate glasses co-doped with erbium and thulium,[12] under 980 nm excitation.

The aims of the present study are to elucidate the role of the rare-earth in governing the structure and properties, including the glass-forming ability, of binary rare-earth titanates. Using containerless processing allows for a more holistic approach, whereby both glasses and high-temperature melts can be studied *in-situ*. Observing the molten state directly allows glass-forming and non-glass-forming compositions to be treated on an equal footing, and as we shall show, yields an improved understanding of the structure-property relationships.

In-situ synchrotron x-ray diffraction and absorption spectroscopy provide detailed and complementary insight into the local structures present, and in particular, to structural changes occurring during (super)cooling and glass formation. Compositions $17RE_2O_3.83TiO_2$, have been chosen, close to the center of the known glass-forming regions of binary lanthanum and neodymium titanates[3] (Table 1). We will make comparison to our analogous studies on glass-forming barium titanate, $BaTi_2O_5$,[13] which has a similar composition of 33.3 cation % Ba, compared to 29.1 cation % RE. The pair distribution functions (PDFs) obtained from high-energy x-ray diffraction revealed a continuous structural transition, whereby both Ti–O and Ba–O coordination numbers increased during cooling and vitrification. Since the rare-earth cations are smaller than Ba^{2+}, an increased overlap of Ti–O and RE–O bond-length distributions can be expected in the x-ray PDFs, and therein lies the utility of the comparison, since signs of similarities or differences in behavior can be sought between $17RE_2O_3.83TiO_2$ and $BaTi_2O_5$, even when resolution of structural features is reduced. To this end, element specific Ti K-edge x-ray absorption near-edge structure (XANES) spectroscopy is shown to be particularly illuminating and complementary.

2. Experimental Details

Materials. Rare-earth oxide fine powders, RE_2O_3 (RE = Sc, Y, La, Nd, Eu, Gd, Ho), Tb_4O_7, Pr_6O_{11}, or CeO_2, of at least 99.9% purity were dried at 873 K for $\gtrsim$ 1 hr before weighing and combining with TiO_2 (Aldrich, 99.99%) in appropriate amounts to yield one gram mixtures of composition $17RE_2O_3.83TiO_2$. Powders were stirred and comingled by tumbling with an alumina mixing bead inside an HDPE bottle. Polycrystalline beads of diameters $\lesssim$ 2 mm, were obtained by 10.6 µm laser hearth melting in a water-cooled copper hearth.[14]

Aerodynamic levitation and laser heating. The rare-earth titanates are relatively refractory, with minimum (eutectic) melting temperatures between 1700 and 1900 K for TiO_2-rich compositions, Table 1. Furthermore, they are relatively reluctant glass formers, and for these reasons a containerless melting technique was selected for studying the liquids *in-situ*, and for increasing the glass forming propensity by elimination of contact with a solid surface. The diffraction, spectroscopic and glass formation tests presented herein all exploit the combination of aerodynamic levitation with laser heating. In a typical experiment a 2 to 3 mm diameter bead of sample material is levitated on a gas stream flowing through a converging-diverging conical nozzle. A 400 W, 10.6 µm, CO_2 laser impinges onto the top of the sample from above, and sample temperature is measured by optical pyrometry in the infrared region.[15, 16]

Glass formation. Tests for glass formation were performed by levitation and heating of ceramic beads up to ~2400 K to ensure complete melting, as ascertained by visual inspection of the sample and video feed, followed by shutting off the laser power. The sample, video feed and pyrometer traces were inspected for signs of recalescence that results from the sudden increase in brightness of a sample when the heat of fusion is released during crystallization of a deeply supercooled liquid. When crystallization was not observed, glass formation was confirmed, or otherwise, by synchrotron x-ray diffraction (see below). When glasses could not initially be obtained, the sample size was progressively reduced in order to yield enhanced cooling rates. Maximum cooling rates are obtained at time of laser shut-off and increased from ~1.0 x 10^3 Ks^{-1} for larger samples, to ~2.0 x 10^3 Ks^{-1} for smaller samples (Fig. 1). At lower temperatures, slower cooling rates are observed, typically of 200 to 600 Ks^{-1} at 1100 K, which is close to T_g. Tests were performed in a levitator nozzle open to the air, initially using pure oxygen gas as the levitation fluid. Where multiple rare-earth valence states are stable, as for cerium (Ce^{4+}, Ce^{3+}), praseodymium (Pr^{4+}, Pr^{3+}) and europium (Eu^{3+}, Eu^{2+}), tests in more reducing high-purity argon and Ar:5%CO gases were also performed. These tests probed the effect of rare-earth valence state changes on the glass formability and glass color, and were later repeated inside a chamber which greatly reduces the influence of air ingestion.

Ti K-Edge X-ray Absorption Spectroscopy. Ti K-edge XANES spectra were collected using beamline 20-BM-B of the Advanced Photon Source (APS, Argonne, IL, USA), as previously described.[13] The beam was unfocussed with a cross-section of 2.5 mm wide by 1.0 mm high. EXAFS regions were not measured in detail since they are strongly damped at high temperatures, while measurement of the XANES region alone allows for shorter measurement times which mitigates against compositional drift due to incongruent volatilization. The chamber enclosing the levitator nozzle included a large x-ray outlet window facing a 13-element Ge detector (Canberra Lege with XIA Xmap electronics) for measuring the fluorescence signal from the sample, perpendicular to the incident beam. Continuously helium purged inserts were used on x-ray inlet and outlet ports to reduce the x-ray path length through the more absorbing chamber gas to *circa* 1 cm prior to absorption by the sample and *circa* 1 cm for the fluorescence signal. Ionization chambers, one upstream and two downstream of the sample position were used to measure transmission through a Ti metal foil for energy calibration (first inflection point of the edge set to 4966.0 eV), as well as for measurements on finely powdered recovered samples mounted on sticky tape.

An energy resolution of $\Delta E/E$ = 1.4 x 10^{-4}, or 0.70 eV at the Ti K-edge, was obtained using a Si(111) double-crystal monochromator. The core-hole lifetime of 0.94 eV[17] yields a total expected peak width after convolution of about 1.3 eV. Spectra were recorded from 150 eV below to 380 eV above the Ti K-edge, with fine, 0.2 eV, steps in the range 15 eV below to 50 eV above the edge. Total measurement time was ~10.33 minutes per spectrum. The absorption length, $\mu(E)$, in melts of $17RE_2O_3.83TiO_2$ composition is ~15 µm below the Ti K-edge (at 4900 eV) and decreases to ~7 µm above the edge (at 5000 eV). The thickness of the samples relative to $\mu(E)$ required the fluorescence intensities to be corrected due to self-absorption. The self-absorption effect arises due to modulation of $\mu(E)$, and thereby the probed volume of the sample, as the x-ray energy is stepped through the edge of interest, and results in a suppression of the spectral features above the edge and an enhancement of the pre-edge region. The larger the contribution of the element of interest to the total absorption coefficient, the larger the effect. Here we

have used the Fluo algorithm[18] available within Athena.[19] Although this correction is applicable to flat-plate sample geometry, we have tested the algorithm on Fe K-edge measurements of a pure iron sphere and compared the results to the transmission measurement through an iron foil. The empirical incident and take-off angles of 45° and 20° ± 10° respectively gave a suitable correction at least up to about 100 eV above the edge.[20] Levitation gas flow was turned off when measuring fluorescence signals from room-temperature beads, in order to reduce motion induced noise of the more irregularly shaped (compared to melts) polycrystalline beads. Temperature was measured with a single-color optical pyrometer (Chino model IRCS) sighted onto the top of the sample where it was also being heated by laser irradiation. The apparent temperature was corrected using a Wien's displacement law approximation[21] with a spectral emissivity value of 0.87 at the 0.9 μm pyrometer wavelength and corrected for reflection losses from a silica window and lens in the optical path.

XANES spectra were corrected and normalized using the IFEFFIT software[22] *via* the Athena interface[19] as described in detail elsewhere.[20, 23] In order to isolate the pre-edge peaks (Fig. 2), two Lorentzian peaks were fitted to the main edge, up to an intensity of ~0.5 normalized units, and with the energy range containing the pre-edge peaks excluded. The isolated pre-edge peaks were then characterized by integrating over the interval $4965.0 \leq E \leq 4972.0$ eV to obtain their total areas, and deriving the first moment of the distribution to yield the centroid position. This was found to give similar, but more robust, results to those obtained by fitting a series of Gaussian lineshapes and excluding those centered at $E >$ 4972.0 eV, Fig. 2b.

Farges *et al*.[24] have previously measured a large number of Ti K-edge XANES spectra for compounds of known structure and shown how pre-edge peak heights and positions correlate with each other, as well as with Ti–O coordination numbers. Here we prefer to use pre-edge peak areas, as defined above, because these, unlike peak heights, do not depend strongly on the energy resolution of the measurements. Farges *et al*.[24] also determined pre-edge peak areas, but did not give sufficient details of their Lorentzian fitting procedure for us to make direct comparison.

High-Energy X-ray Diffraction. X-ray diffraction measurements were made at beamline 6-ID-D of the APS using 100.23 keV x-rays, as described previously.[13] Diffraction patterns were collected during isothermal 60 s holds of molten $17La_2O_3.83TiO_2$ during stepwise cooling, and a 300 s measurement on a quenched glass bead was made for comparison. Reported melt temperatures were averaged over each 60 s measurement window. Measured mass losses imply negligible compositional drift for any of the samples. An x-ray large-area detector (Perkin Elmer XRD1621, 2048 x 2048 pixels of 200 μm x 200 μm Tl doped CsI) was used with 332.0 mm sample-to-detector distance, calibrated using the powder diffraction pattern of NIST standard CeO_2. Temperature was measured using 5 μm wavelength optical pyrometry, the long wavelength being chosen to avoid near-infrared transparency of the melts at the lower temperatures investigated. Apparent temperature was corrected using a Wien's displacement law approximation[21] with a spectral emissivity value of 0.88 estimated from the Fresnel losses for a material with a refractive index of 2.05.[25] The pyrometer temperature was also corrected for reflection losses from a CaF_2 window and lens that were in the optical path. The diffraction data reduction and definitions of the scattering functions used are given elsewhere.[26, 27, 28] The measured structure factors, $S(Q)$, represented as functions of $Q = (4\pi\sin\theta)/\lambda$, with 2θ the scattering angle, and $\lambda = 0.12370$ Å the x-ray wavelength, were Fourier

transformed with Q_{max} = 20 Å^{-1}, without modification (window) function. An additional transform with Q_{max} = 23 Å^{-1} was made of the glass measurement, yielding improved resolution, enabled by the improved signal-to-noise of the longer measurement, and the reduced Debye-Waller damping at room temperature.

Quantification of the local cation-oxygen coordination environments was achieved by sequential peak fitting[29] to the leading edge of the main Ti–O peak in $T(r)$, followed by the leading edge of the main La-O peak in the residual, and finally by fitting of a 2nd Ti–O peak, at longer interatomic distance, to the remaining residual.

Melt Densities. Quantitative analysis of total scattering diffraction data requires knowledge of the atom number density. Since no measurements are available for $17La_2O_3.83TiO_2$ melts, the density-temperature relation was estimated based on: i) the density of the glass, 4.84 gcm^{-3}, as interpolated from existing measurements;[6] ii) an estimated volume thermal expansion coefficient for the glass of 4.0 x 10^{-5} K^{-1},[30] up to the interpolated glass transition temperature of 1082 K;[6] iii) a liquid density temperature coefficient of –3.4 x 10^{-4} gcm^{-3} K^{-1} consistent with other titanate melts,[13, 31, 32, 33] equivalent to a volume thermal expansion coefficient for the melt of between 7 and 8 x 10^{-5} K^{-1}.

3. Results

Rare-Earth Titanate Glass formation. Glass formation was confirmed by aerodynamic levitation and laser heating in oxygen gas flows for lanthanum and neodymium titanates of the $17RE_2O_3.83TiO_2$ composition, in accord with previous reports, Table 1.[1, 3, 6] By the same means, new glasses were found of europium (orange, ≤ 13.7mg) and gadolinium (clear, ≤ 9.2mg) titanates of the same nominal composition. Exemplary cooling traces from pyrometry and photographs of the glass beads obtained are shown in Fig. 1. No glass formation was observed for the smaller rare-earths, scandium, yttrium, terbium or holmium titanates. In oxygen gas flow, no glasses of cerium or praseodymium titanate were obtained. In argon gas flow, praseodymium titanate droplets were quenched to form dark glass beads (Fig. 1) of 10.2 mg in a nozzle open to air, and 16.5 mg in the enclosed chamber. No glasses of cerium titanate were similarly obtained. Europium titanate also formed glasses in both argon and Ar:5%CO, but rather than taking an orange color, these beads are very dark, perhaps green (Fig. 1). Notably, these reduced Eu titanate glasses only formed in the levitator open to air ingestion, and not when enclosed inside a chamber. Further investigation inside a sealed chamber revealed glass formation in pure oxygen down to 5%O_2 in argon.

Ti K-Edge XANES. Pre-edge regions of the Ti K-edge XANES spectra are plotted in Fig. 2. Comparison of the spectra obtained from lanthanum titanate melt and glass in Fig. 2a reveal broadening of the main edge, alongside an increase in pre-edge peak intensity and a slight shift to lower energy in the liquid phase. A very similar change is observed for the neodymium titanate liquid upon glass formation (Fig. 2c and 2d). These observations are consistent with an increase in the average Ti–O coordination number during cooling of the melts and subsequent vitrification,[13, 24, 34] similar to that observed, and confirmed by high-energy x-ray diffraction, for $BaTi_2O_5$.[13] Spectra obtained for all four rare-earth titanate melts are compared in Fig. 2c, and these reveal a gradual decrease in pre-edge intensity as the rare-earth cation size decreases

from La to Sc. The polycrystalline products of quenches from Y and Sc titanate liquids display smaller pre-edge features, Fig. 2d, than do the glasses or melts. This is to be expected based on the equilibrium phase diagrams,[35, 36] which predict mixtures of rutile TiO_2 with Sc_2TiO_5 or pyrochlore $Y_2Ti_2O_7$, all of which contain Ti in octahedral environments only. The actual phases present have not been confirmed.

The results of pre-edge peak integrations, as illustrated in Fig. 2b, are listed in Table 2 and plotted in Fig 3a. Also shown in Fig. 3 are data obtained in an identical fashion from liquid and glassy $BaTi_2O_5$,[13] and molten $BaTiO_3$.[28] Using the published coordination numbers derived from HEXRD for barium titanate liquids and glasses, along with crystallographic values for polycrystalline quench products, it is possible to calibrate the total pre-edge area against n_{TiO}, and to thereby predict n_{TiO}. Based on the limited number of data (N = 9), a simple linear interpolation (Fig. 3b) yields

$$n_{\mathrm{TiO}} = n_{\mathrm{TiO}}^{0} - kA,$$

with A the pre-edge peak area as defined above (Fig. 2b) and (n_{TiO}^{0} , k) = (6.60(80), 1.43(13) eV^{-1}). Using HEXRD results for $17La_2O_3.83TiO_2$ presented below yields a slightly different result, (n_{TiO}^{0} , k) = (6.70(77), 1.76(15) eV^{-1}). We suggest the most reliable correlation is that shown in Fig. 3c using the combined datasets (N = 15), with (n_{TiO}^{0} , k) = (6.64(65), 1.56(12) eV^{-1}). Predicted coordination numbers thus obtained are given in Table 2. Note that the fluorescence measurements on glass beads tend to yield pre-edge peak areas 5 to 10% larger than obtained by powder transmission, which likely implies that the self-absorption correction applied was not quite large enough. For the La titanate glass bead, a value n_{TiO} = 5.5(2) is obtained, or n_{TiO} = 5.6(1) from the powder transmission spectrum. These measurements are in reasonable agreement with the published result of n_{TiO} = 5.35 obtained from a combination of neutron diffraction and HEXRD,[6] and are compared to our HEXRD results below. For the melts a gradual increase from n_{TiO} = 4.8(2) for La through n_{TiO} = 4.9(2) for Nd and Y, to n_{TiO} = 5.1(2) for molten Sc titanate is implied.

It is worth noting that the result for molten La titanate in a highly reducing Ar:5%CO atmosphere is not distinguishable from that in pure oxygen gas. This suggests that any reduction of $Ti^{4+} \rightarrow Ti^{3+}$ on the timescale of the experiment is below the detection limit of the XANES measurements (few %). Nonetheless, a tiny fraction of Ti^{3+} is implied by the darkening of the sample and its crystallization, as opposed to vitrification, upon quenching. This result is completely analogous to observations made for $BaTi_2O_5$.[13]

Our results are qualitatively consistent with previous observations of correlations between pre-edge peak parameters and Ti–O coordination numbers.[24] However, we reiterate that we favor the use of pre-edge peak areas, as opposed to peak heights, because the former do not depend strongly on the energy resolution of the measurements. Previously reported pre-edge peak areas are not necessarily directly comparable to ours due to different, and ill-defined, methods of determination.[24] Furthermore, the wide temperature range covered by our measurements may introduce an additional influence on the pre-edge peak areas due to increased thermal disorder, such that slightly different correlations to those plotted in Fig. 3 may be obtained if only room temperature measurements were included (see also Final Remarks in the Discussion section).

High-Energy X-ray Diffraction. Selected diffraction patterns obtained for molten and glassy lanthanum titanate are plotted in Fig. 4, and their sine Fourier transforms in Fig. 5. There is stark contrast between the glass and the liquids, but only subtle changes between the high temperature melt and the supercooled liquid (SCL), despite the almost 500 K temperature difference. The medium range structure apparent in Fig. 5a, for $5 \lesssim r \lesssim 12$ Å, clearly shifts to longer distances in the melt *cf*. the glass, consistent with bulk thermal expansion, and is a manifestation of the first diffraction peak (Fig. 4), which shifts to smaller Q values in the liquid. On the other hand, the bonded metal-oxygen peaks actually shift to shorter distances in the melts (Fig. 5), a phenomenon observed for other glass-forming oxide liquids,[37, 38, 39, 40] including barium titanate,[13] and suggestive of smaller coordination numbers in the melt.

Results of peak fitting to $T(r)$ are recorded in Tables 3 and 4, with some exemplary fits plotted in Fig. 6. Results for the glass are in good agreement with a previous neutron diffraction and HEXRD study[6] of $La_4Ti_9O_{24}$ glass, which is slightly richer in lanthanum (18.18 mol% La_2O_3) than our material. Although the peak fitting procedure differed, and the O–O correlation was eliminated in the published work, we find excellent agreement in the mean values for the Ti–O distance, $\langle r_{TiO} \rangle$, and Ti–O coordination, $\langle n_{TiO} \rangle$, Table 4. The fact that the two individual Ti–O peaks differ is not considered important given the arbitrary nature of fitting multiple symmetric contributions to characterize an asymmetric distribution. We find a large La–O coordination of $n_{LaO} = 9.6(3)$, compared to the previous work ($n_{LaO} = 8.0$)[6]. This is likely due to a small contribution from O–O correlations in our La–O peak fit, but also due to the higher r peaks included in the fitting in Ref.[6]. As such, a value of $n_{LaO} > 8$ is quite likely, especially given the fact that the residual in Fig. 6b and 5e includes not only O–O distances, but likely longer La–O distances as well, which is supported by the existence of intensity in this region in the published x-ray-neutron difference function with O–O peaks eliminated.[6]

Unique fits to the second Ti–O peak (Ti–O(2)) and the La–O peak in the liquids could not be obtained owing to their strong overlap, see the residual in Fig. 6c. In order to estimate their positions and coordination numbers, mean values were taken over the widely varying fits obtained for each of the five liquid diffraction patterns. These mean values are recorded in the final row of Table 4, with standard deviations in parentheses. The behavior appears similar to that observed in molten $BaTi_2O_5$,[13] where the fact that the Ba–O bonds are about 0.1 Å longer than the La–O bonds observed herein provided just enough separation from the Ti–O peaks to enable more detailed fitting. The main conclusion is that the Ti–O coordination is smaller in the melts than in the glass, a result which is consistent with the information derived from Ti K-edge XANES spectra. A reduction in La–O coordination is also apparent, although this is not as drastic as that observed for Ba–O,[13] which is likely related to the higher field strength of lanthanum. Although the n_{TiO} values obtained by diffraction are similar, it is interesting to note that the Ti–O coordination appears to be slightly higher in the rare-earth titanate liquids and glasses than in the barium titanate, $BaTi_2O_5$.[13] This is supported by the longer Ti–O modal bond lengths in the RE titanate, Fig. 7, as well as by the XANES observations. Furthermore, both La and Ba modifier oxides appear to suppress n_{TiO} compared to its value in pure molten TiO_2,[27] which is again supported by comparison of the modal bond lengths, Fig. 7.

Results of fitting to the first diffraction peaks are recorded in Table 3 and plotted in Fig. 8 in terms of the associated real-space length scales. The periodicity $l_1 = 2\pi/Q_1$ increases from 3.01(1) Å in the glass to

3.13(2) Å in the high temperature melt, qualitatively consistent with expected bulk thermal expansion. These periodicities can be seen in the $D(r)$ functions of Fig. 5a, beyond the first cation-cation peak(s) *circa* 3.5 to 4.0 Å. The fact that the l_1 periodicities are ∼5% shorter than in $BaTi_2O_5$ can be rationalized on the basis that the La–O bonds are a similar amount shorter than the Ba–O bonds. This leads to shorter Ti–La (*cf*. Ti–Ba) distances, and it is these Ti–La correlations that likely dominate the first diffraction peak, since they are the most strongly weighted in the x-ray diffraction patterns, of the six unique atom pair terms present. Similarly, the atom number densities in $17La_2O_3.83TiO_2$ are ∼12% larger than in $BaTi_2O_5$, comparable to the ∼16% larger Q_1^3 values.

The correlation lengths $\xi_1 = 2\pi/\Delta Q_1$ plotted in Fig. 8b characterize the decay of the high r oscillations seen in the $D(r)$ functions of Fig. 5a. Naturally, the ordering extends out further at lower temperatures. Again, as for the l_1, the ξ_1 appear slightly shorter than in the Ba titanate, however, this leads to essentially identical values for the number of ordered cation-cation shells, ξ_1/l_1, which decays from 3.92(3) (4.02(3)) in the La (Ba) glass to 2.45(2) (2.41(2)) in the hottest La (Ba) melt.

It is instructive to note the influence of the maximum scattering vector magnitude, Q_{max}, on the resolution of the real-space functions in Fig. 6. For the glass, measurement duration was sufficiently long and Debye-Waller factors sufficiently small, compared to the liquids, that additional information is contained in the measured $S(Q)$ beyond 20 $Å^{-1}$. As can be seen from comparison of Fig. 6a with 6d (and 6b with 6e), a 15% increase in Q_{max} yields resolution of a peak in the residual (Fig. 6d) as well as a peak at 2.97(1) Å which was not previously resolved.[6] The first of these is attributed to longer Ti–O bonds, while the 2.97(1) Å peak likely arises from a combination of longer La–O bonds and non-bonded O–O distances. Fitting to the higher resolution $T(r)$ yields similar results (Table 4), although notably the Ti–O coordination increases slightly to 5.46(9), which is more closely in accord with XANES estimates (Table 2) and the fact that XANES indicates a higher Ti–O coordination in the La titanate glass compared to the Ba titanate. The latter point is also consistent with previous diffraction studies on the two glasses.[6, 41]

4. Discussion

Influence of Structural Basicity on Structure. The utility of *in-situ* measurements on molten materials is demonstrated in several ways by the dataset presented herein. A key advantage is that both glass-forming and non-glass-forming materials can be treated on an equal footing. This capability has revealed an effect of the rare-earth cation size on the Ti–O network, something which may not have been possible based on the glasses alone. In particular, the smaller RE elements appear to increase the Ti–O coordination, something which can be expected to contribute to the reduced glass-forming ability of titanate melts bearing the smaller rare-earth cations. An analogous effect is seen in rare-earth aluminates and aluminosilicates,[42] and has also been observed for alkali titanate glasses, whereby the larger alkali modifier cations give rise to smaller Ti–O coordination numbers.[43, 44, 45, 46] Indeed, it has been suggested that, in general, increasing the structural basicity parameter (Λ_S) of titanate glasses causes the Ti–O coordination to decrease,[43] where structural basicity is the product of molar modifier formal charge content ($x(M_{2/Z}O)$) with inverse modifier potential (r_M/Z_M), i.e.

$$\Lambda_S = x(M_{2/Z_M}\mathrm{O}).\frac{r_M}{Z_M} \sim \Lambda_0 - Kn_{\mathrm{TiO}}$$

where Z_M is the formal oxidation state, Λ_0 and K are positive constants. We note that this definition of basicity is related to, but clearly distinct from, the optical basicity[47] commonly used in glass science. The $\sim$ symbol is used for the right-hand side of the equation to indicate a scaling relation, as opposed to a true equality, because Yoshimaru *et al*.[43] actually observed a non-linear dependence of n_{TiO} on Λ_S. Our data are consistent with this hypothesis, which furthermore explains the larger n_{TiO} in the rare-earth titanates, as compared to the corresponding $BaTi_2O_5$ melts and glasses. Additional support comes from recent x-ray and neutron diffraction, and Ti XANES measurements on molten $BaTiO_3$ – the increase in structural basicity with added BaO content further suppresses n_{TiO} down to a value of 4.4(2) at *circa* 2100 K.[28] This latter value is in excellent agreement with our empirical relationship between Ti K-edge pre-edge peak area and Ti–O coordination, which predicts n_{TiO} = 4.3(2), Fig. 3. This demonstrates the advantage of a description based on Λ_S, as opposed to only cation potential or field strength, because effects of both bulk composition and modifier cation size/charge are included.

It is interesting to note that the dependence of n_{TiO} on Λ_S does *not* appear to explain the observed temperature dependence of $n_{\mathrm{TiO}}(T)$. Our data demonstrate structural differences between melts and their quenched products, both vitreous and crystalline. These imply dramatic rearrangements of the supercooled liquids, not only upon crystallization, but also during cooling and glass formation. In particular, n_{TiO} tends to decrease with increasing T, or *vice versa*. The structural basicity of the melt can be considered to depend on temperature through the modifier cation radius, $\Lambda_S(T) = xM_{2/Z}\mathrm{O}.(r_M(T)/Z_M)$. Thus, to drive the observed Ti–O coordination decreases in titanate melts with increasing temperature, the modifier cation radius, and therefore bond lengths and coordination numbers, should increase. This is exactly the opposite of what the available evidence suggests for La and Ba modifiers. It furthermore cannot explain the temperature dependence of $n_{\mathrm{TiO}}(T)$ in pure molten TiO_2.[27] Therefore, the relationship between Ti–O coordination and structural basicity is not completely general. Indeed, it does not appear to hold for large additions of silica, where very high proportions of tetrahedral Ti are evidenced in silica-rich SiO_2–TiO_2 glasses,[48] although this could be related to the very high fictive temperature of such glasses.

Rare-Earth Titanate Glass Formation. Our observations of new glasses formed from europium and gadolinium titanate melts extend the range of glass formation along the rare-earth series, from the previously reported glasses containing the largest RE cations, toward rare-earths with progressively smaller radii. It is also clear from the sizes of samples obtained, and the eventual lack of glass formation, that glass formability decreases with the RE cation radius. This observation is similar to that for binary rare-earth aluminates, where the glass forming ranges progressively narrow as the RE cation reduces in size.[49] Similarly for alkali and alkaline-earth titanates, the glass forming regions are wider in the presence of the larger modifier cations.[43] We hypothesize that titanate melts containing combinations of rare-earths, e.g. $17(RE,RE',RE'',\ldots)_2O_3.83TiO_2$, will form glass so long as the mean cation radius is larger than that of gadolinium, $\langle r_{RE}\rangle \gtrsim r_{Gd}$. This certainly appears to be the case for reported examples, including La-Yb titanate-zirconate glasses doped with Ho,[50] or co-doped with Er-Tm[12] ($\langle r_{RE}\rangle \gtrsim r_{Pm}$), and for La-Gd titanate glasses[4] ($\langle r_{RE}\rangle \gtrsim r_{Pr}$). It is quite possible that glasses of Tb (or even smaller RE) titanate could be formed with enhanced cooling rates.

The results of our glass formation tests are consistent with early roller-quenching studies[2] which showed glass formation for $20La_2O_3.80TiO_2$ and $20CeO_2.80TiO_2$, but failed to obtain any glasses for Y_2O_3–TiO_2 compositions with 15 to 20 mol% Y_2O_3 (see also Ref.[1]). In oxygen gas flow, no glasses of cerium or praseodymium titanate were obtained by us, implying that the presence of a fraction of tetravalent rare-earth cations is deleterious to glass formation. In argon gas flow, praseodymium titanate glass was obtained, whilst cerium titanate crystallized. Since Ce^{4+} is more stable than Pr^{4+}, this supports the supposition that the tetravalent rare-earths tend to hinder glass formation in the present titanate compositions. Indeed, oxidizing $RE^{3+} \rightarrow RE^{4+}$ also decreases the structural basicity of the melt, which could increase the Ti–O coordination and decrease glass formability, as discussed above. The fact that '$20CeO_2.80TiO_2$' glass has been formed by roller-quenching[2] indicates that much faster cooling rates, $\sim 10^5$ Ks^{-1}, are required than obtained for levitated droplets. Cooling rates for levitated droplets vary with time and temperature (Fig. 1a), typically from $\gtrsim 10^3$ Ks^{-1} at time of laser shut-off, to several hundred Ks^{-1} at the glass transition temperatures, and these rates increase as sample size decreases. Glass-forming propensity in containerless conditions is typically enhanced by elimination of heterogeneous crystal nucleation at a melt-container interface (or from dissolved impurities from a solid container) and this can lead to lower critical cooling rates.[51] For the case of Ce titanate, it appears that faster cooling is the more important factor.

The observed coloration of the Eu titanate beads (Fig. 1b) is reasonably consistent with those of europium aluminosilicate glasses formed in oxidizing (air) and reducing (N_2) atmospheres,[52] and reflects a shift from $Eu^{3+} \rightarrow Eu^{2+}$. The formation of Eu titanate glass in reducing Ar or Ar:5%CO levitation gases was only possible in the presence of some ingestion of air into the gas surrounding the sample. We therefore conclude that oxidizing or *mildly reducing* atmospheres permit Eu titanate glass formation. It is interesting to note that the largest (fully amorphous) glass bead was obtained under mildly reducing conditions. This implies that formation of some Eu^{2+} may in fact enhance the glass formability. Indeed, reduction of $RE^{3+} \rightarrow RE^{2+}$ increases the structural basicity of the melt, which is expected to decrease the Ti–O coordination and increase the glass formability, as discussed above. We note that Eu^{2+} has a similar cation radius to Sr^{2+}, and a wide range of mixed rare-earth-heavy-alkaline-earth titanate glasses have been reported.[4, 41] Formation of a redox couple, whereby $Eu^{3+} + Ti^{3+} \rightleftharpoons Eu^{2+} + Ti^{4+}$, may also play an important role in eliminating Ti^{3+} crystal nucleation sites.

Titanate Glass Formation. On the subject of titanate glass forming ability, an important observation can be made in light of the measured Ti–O coordination numbers and glass-forming composition ranges. Specifically, the glass-forming ranges always include compositions for which the mean O–Ti coordination is two. Bond counting leads to the general relationship

$$n_{\mathrm{OTi}} = (c_{\mathrm{Ti}}/c_{\mathrm{O}})n_{\mathrm{TiO}},$$

where c_i are atom fractions. Thus for rare-earth titanates, $x_{\mathrm{RE}}RE_2O_3.(1 - x_{\mathrm{RE}})TiO_2$,

$$n_{\mathrm{OTi}} = \frac{1-x_{\mathrm{RE}}}{2+x_{\mathrm{RE}}} n_{\mathrm{TiO}}.$$

From this it can be seen that the glass forming regions (Table 1) bracket the composition for which $n_{\mathrm{OTi}} = 2$ for La and Nd titanate glasses, so long as $5.0 \lesssim n_{\mathrm{TiO}} \lesssim 5.5$, which is consistent with our HEXRD determination herein, and with the published results.[6] The Sm titanate glass composition for which glass formation is reported[5] has $n_{\mathrm{OTi}} \simeq 2.0$. Thus, compositions with $n_{\mathrm{OTi}} \simeq 2.0$ appear to be the most stable glasses, which seems reasonable because for this value a continuous Ti–O network can exist, with only bridging oxygen (OTi_2), and free from triclusters (OTi_3) or non-bridging oxygen (OTi_1). Alternatively, it may be sufficient that the number of OTi_3 and OTi_1 are equal (at $n_{\mathrm{OTi}} \simeq 2.0$) and thereby charge-balance each other. Triclusters can be considered to limit glass formation due to promotion of edge-sharing and reducing the topological degrees of freedom, whilst non-bridging oxygen are associated with depolymerization of the Ti–O network, and lower glass forming ability. Furthermore, the existence of eutectics (Table 1) close to the $n_{\mathrm{OTi}} \simeq 2.0$ compositions for the rare-earth titanates also suggests that melts with this configuration are more stable, with lower free energies, which goes hand-in-hand with glass formation. We therefore assert that triclusters in the titanate glasses limit glass formation in a topological manner, by limiting the ability to form a disordered Ti–O network. Of course, given the finite glass forming ranges, some OTi_3 are clearly permitted, as are some OTi_1. For the RE titanate glasses O–Ti coordination falls in the range $1.9 \lesssim n_{\mathrm{OTi}} \lesssim 2.1$, implying at least ~10% OTi_1 or OTi_3.

The above idea can be extended to alkali and alkaline-earth titanate glasses, where it again appears that glass formation occurs around the $n_{\mathrm{OTi}} \simeq 2.0$ composition(s), but with increased glass forming ranges, implying increased OTi_3 and OTi_1 solubilities. For $x_M M_{2/Z}O.(1 - x_M)TiO_2$ (Z = 1,2) compositions

$$n_{\mathrm{OTi}} = \frac{1-x_{\mathrm{M}}}{2-x_{\mathrm{M}}} n_{\mathrm{TiO}}.$$

Values for n_{TiO} for Na, K, Rb and Ba titanate glasses can be calculated from the photoacoustic spectroscopy data of Yoshimaru *et al*.[43]. Notably the values obtained for Ba titanate glasses agree very well with our HEXRD and published results.[13, 41] Taking the reported glass forming regions from the same report[43] and calculating O–Ti coordination numbers yields values $1.5 \lesssim n_{\mathrm{OTi}} \lesssim 2.5$, a much wider range than for the RE titanates. This could be a result of the different glass production methods, containerless aerodynamic levitation for the RE titanates, and more rapid splat quenching for the glasses of Yoshimaru *et al*.[43]. Nonetheless, the glass forming regions again center around the $n_{\mathrm{OTi}} \simeq 2.0$ composition(s), supporting our claim that this is the optimal structure for glass formation topologically.

One should also bear in mind that local configurations in the melt similar to those observed in the crystalline phases do not necessarily lead to crystal nucleation. Indeed, the 'best' glass formers, such as SiO_2, often have the same local structures as their crystalline forms, such that their free energies are as close as possible. It is therefore interesting to note that the RE titanates which form glasses most easily (RE = La and Nd) also form crystalline phases with compositions close to the glass forming eutectic (Table 1). Specifically, $La_4Ti_9O_{24}$ and $Nd_4Ti_9O_{24}$ are both within the glass forming ranges, which means that liquids and glasses can potentially form with free energies close to those of the equilibrium phase assemblages. Such a situation is less likely for the majority of RE titanate systems where the pyrochlore, $RE_2Ti_2O_7$, crystal stoichiometry is the most Ti-rich RE-bearing phase, or for Sc titanate where even the pyrochlore structure is unstable and Sc_2TiO_5 is the most Ti-rich Sc-bearing phase (Table 1).

Final Remarks. The empirical linear relationship derived between n_{TiO} and Ti K-edge pre-edge peak area, *A* (Fig. 3), has some limitations. For one, it cannot predict coordination numbers larger than n_{TiO}^{0} (the *A* = 0 limit), and, at best, should be expected to give reliable results only within the typical (ambient-pressure) range of $4 \lesssim n_{TiO} \lesssim 6$. Furthermore, it does not account for the considerable variations in *A* arising from polyhedral distortion at fixed n_{TiO}. Nonetheless, given the broad distributions of local coordination environments in melts and glasses, the calibration of the relationship using HEXRD information on such materials should make it suitable for application in similarly disordered systems, as appears to be the case. Future work will involve using additional HEXRD data to derive more reliable fitting parameters, (n_{TiO}^{0} , *k*) and to separate the effects of possible thermally induced distortion[53] from those of coordination change.

We are confident in our observed trend in pre-edge peak area with RE cation size, Fig. 3a, despite the relative subtlety of the effect. This is based on the fact that a large portion of the error bars plotted are due to systematic effects, as opposed to purely random statistical variations. In particular, an uncertainty of 10% in *A* is ascribed to the interpolation and subtraction of the main edge contribution prior to integration, and this is largely systematic. Our result could be verified with further diffraction measurements on RE titanate melts bearing the smaller RE cations, either by exploiting Y-Ho isomorphism with HEXRD,[40] or Ti isotope substitution in neutron diffraction.[28] Such measurements would additionally discriminate between competing interpretations. For example, the observed variation in *A* might be explained by increased distortion of Ti–O polyhedra as the RE cation size decreases, conceivably without any change in average Ti–O coordination number.

5. Conclusions

Molten rare-earth titanates with composition $17RE_2O_3.83TiO_2$ have been obtained within an aerodynamic levitation furnace coupled with 10.6μm laser heating. Glass formation has been confirmed for the larger rare-earth La and Nd titanates in an oxygen gas flow, and extended to include the smaller rare-earth Eu and Gd titanates. Eu and Pr titanate glasses were also obtained in mildly reducing conditions. Glasses were not obtained for Sc, Y, Ho, Tb or Ce titanates, and a reducing CO-bearing atmosphere prevents glass formation even in the La titanate, likely due to formation of a small number of Ti^{3+} defects.

The levitated liquid droplets were examined *in-situ* by Ti K-edge x-ray absorption near-edge structure (XANES) spectroscopy at the Advanced Photon Source, in the 1900 to 2060 K temperature range. An effect of the rare-earth cation potential on the Ti–O environments was observed. In particular, reducing the RE cation radius leads to an increase in Ti–O coordination number. This result is consistent with existing evidence from alkali and alkaline-earth titanate glasses, whereby Ti–O coordination tends to decrease with increasing structural basicity of the glass, that is, with either or both the modifier cation radius/charge ratio and/or modifier content increasing. The concept of the influence of overall structural basicity on local coordination of titanium is thereby extended to the trivalent rare-earth modifiers, and to the liquid state. This result would have been difficult to obtain without *in-situ* measurements, i.e. using glasses alone, due to the lack of glass formation for the smaller RE titanates. Indeed, this effect of structural basicity on Ti–O coordination is implicated in governing the diminishing glass forming ability as RE cation size decreases, just as the glass forming region for alkali titanates narrows for Na, compared to the larger alkali cations, and disappears altogether for Li.[46]

Comparison of the pre-edge peaks of Ti K-edge XANES spectra for the melts to those for the quench products reveals that Ti–O coordination is smaller in the liquids, as compared to both the crystalline solids (octahedral coordination) and to the glasses. This implies large structural rearrangements not only during crystallization, but also during supercooling and vitrification, similar to observations for barium titanate glass formation.[13] Calibration of XANES pre-edge peak areas to Ti–O coordination (n_{TiO}) measured directly by high-energy x-ray diffraction in barium titanate melts and glasses allows estimation of n_{TiO} in the RE titanates. By this method, n_{TiO} is seen to increase from 4.8(2) in molten La titanate to 5.1(2) in molten Sc titanate. Furthermore, upon quenching and glass formation in Nd and La titanates, n_{TiO} increases to about 5.5(1), or by about 15%.

By analogous means of levitation and laser heating, $17La_2O_3.83TiO_2$ was studied *in-situ* by HEXRD, between 1930 and 1460 K, which is down to an undercooling of 260 K, or about 15% below the melting point. The results support the conclusions obtained from XANES spectroscopy. In particular, the Ti–O bond lengths and coordination numbers are smaller in the liquid state, $n_{TiO} \simeq 4.7(2)$, as compared to the glass, $n_{TiO} = 5.5(1)$.

HEXRD evidence indicates that, as for Ti–O, the La–O (and Ba–O) coordination likely also decreases with increasing temperature. This temperature dependence is not explained by the structural basicity concept, because the resulting decreasing modifier radius with increasing temperature should cause structural basicity to decrease and Ti–O coordination to increase, opposite to observations.

Finally, we note that glass forming regions for titanate glasses bearing monovalent, divalent and trivalent modifier cations all center around compositions where the mean O–Ti coordination number is two. We therefore suggest that the most stable titanate glass structures have $n_{OTi} \simeq 2.0$, where a continuous Ti–O network can be built from bridging oxygen (OTi_2), charge balanced by modifier cations, with minimal non-bridging oxygen (OTi_1) or oxygen triclusters (OTi_3). Or alternatively, that the number of OTi_3 and OTi_1 are equal (at $n_{OTi} \simeq 2.0$) and thereby charge-balance each other.

Acknowledgements

Dr. Steve Heald and Samuel Sendelbach are gratefully acknowledged for help with XANES measurements and sample preparation, and Charlie Weiss and Emma Clark for sample preparation and glass formation testing. Work was supported by U.S. Department of Energy (DOE) under grant number SBIR DE-SC0015241 and DE-SC0018601 (OLGA, AJT, JKRW) and sample preparation and glass formation testing partially supported by NASA grant number 80NSSC19K0518. This research used resources of the Advanced Photon Source, a U.S. DOE Office of Science User Facility operated for the DOE Office of Science by Argonne National Laboratory under Contract No. DE-AC02-06CH11357.

References

1. Kozuka H, Ota R, Soga N. Preparation and properties of binary oxide glasses containing rare earth oxides. *J. Soc. Mater. Sci., Jpn.* 1986; 35(388): 73-79.
2. Suzuki T, Anthony A-M. Rapid quenching on the binary systems of high temperature oxides. *Mater. Res. Bull.* 1974; 9(6): 745-753.

3. Kaneko M, Yu J, Masuno A, Inoue H, Vijaya Kumar MS, Odawara O, et al. Glass Formation in $LaO_{3/2}$–TiO_2 Binary System by Containerless Processing. *J. Am. Ceram. Soc.* 2012; 95(1): 79-81.
4. Masuno A, Watanabe Y, Inoue H, Arai Y, Yu J, Kaneko M. Glass-Forming Region and High Refractive Index of TiO_2-Based Glasses Prepared by Containerless Processing. *Phys. Status Solidi C.* 2012; 9(12): 2424-2427.
5. Maruyama K, Arai Y, Sato S, Sanada M, Otomo T, Suzuya K, et al. Neutron Diffraction Study of Isotope Enriched Glassy $Sm_4Ti_9O_{24}$. pp. 031007 in Proceedings of the 2nd International Symposium on Science at J-PARC Unlocking the Mysteries of Life, Matter and the Universe. Vol. 8.
6. Arai Y, Itoh K, Kohara S, Yu J. Refractive index calculation using the structural properties of $La_4Ti_9O_{24}$ glass. *J. Appl. Phys.* 2008; 103(9): 094905.
7. Laube M, Rauch F, Ottermann C, Anderson O, Bange K. Density of thin TiO_2 films. *Nucl. Instrum. Meth. B.* 1996; 113(1-4): 288-292.
8. Mergel D, Buschendorf D, Eggert S, Grammes R, Samset B. Density and refractive index of TiO_2 films prepared by reactive evaporation. *Thin Solid Films.* 2000; 371(1–2): 218-224.
9. Edwards DF, Ochoa E. Infrared refractive index of diamond. *J. Opt. Soc. Am.* 1981; 71(5): 607-608.
10. Li X, Ma X, Li J, He G, Li J. Synthesis of amorphous $La_4Ti_9O_{24}$ microspheres with high-refractive index via containerless flame-spraying method. *Mater. Res. Bull.* 2018; 97: 567-571.
11. Darafsheh A, Walsh GF, Dal Negro L, Astratov VN. Optical super-resolution by high-index liquid-immersed microspheres. *Appl. Phys. Lett.* 2012; 101(14): 141128.
12. Zhang M, Yu J, Jiang W, Liu Y, Ai F, Wen H, et al. Bright white upconversion luminescence from Er^{3+}/Tm^{3+}/Yb^{3+}-doped titanate-based glasses prepared by aerodynamic levitation method. *Opt Mater.* 2017; 72: 447-451.
13. Alderman OLG, Benmore CJ, Tamalonis A, Sendelbach S, Heald SM, Weber R. Continuous Structural Transition in Glass-Forming Molten Titanate $BaTi_2O_5$. *J. Phys. Chem. C.* 2016; 120(47): 26974–26985.
14. Weber JKR, Felten JJ, Nordine PC. Laser hearth melt processing of ceramic materials. *Rev. Sci. Instrum.* 1996; 67(2): 522-524.
15. Weber JKR, Tamalonis A, Benmore CJ, Alderman OLG, Sendelbach S, Hebden A, et al. Aerodynamic Levitator for In Situ X-ray Structure Measurements on High Temperature and Molten Nuclear Fuel Materials. *Rev. Sci. Instrum.* 2016; 87: 073902.
16. Weber J, Benmore C, Skinner L, Neuefeind J, Tumber S, Jennings G, et al. Measurements of Liquid and Glass Structures Using Aerodynamic Levitation and In-Situ High Energy X-ray and Neutron Scattering. *J. Non-Cryst. Solids.* 2014; 383: 49-51.
17. Krause MO, Oliver J. Natural Widths of Atomic K and L Levels, Kα X-ray Lines and Several KLL Auger Lines. *J. Phys. Chem. Ref. Data.* 1979; 8(2): 329-338.
18. Haskel D. FLUO: Correcting XANES for Self-Absorption in Fluorescence Measurements. *Computer program and documentation [online]. Available from http://www.aps.anl.gov/xfd/people/haskel/fluo.html (accessed January 4, 2009).* 1999.
19. Ravel B, Newville M. ATHENA, ARTEMIS, HEPHAESTUS: Data Analysis for X-ray Absorption Spectroscopy Using IFEFFIT. *J. Synchrotron Radiat.* 2005; 12(4): 537-541.
20. Alderman OLG, Wilding MC, Tamalonis A, Sendelbach S, Heald SM, Benmore CJ, et al. Iron K-edge XANES Spectroscopy of Aerodynamically Levitated Silicate Melts and Glasses. *Chem. Geol.* 2017; 453: 169-185.
21. Weber JKR, Krishnan S, Anderson CD, Nordine PC. Spectral absorption coefficient of molten aluminum oxide from 0.385 to 0.780 μm. *J. Am. Ceram. Soc.* 1995; 78(3): 583-587.
22. Newville M. IFEFFIT: Interactive XAFS Analysis and FEFF Fitting. *J. Synchrotron Radiat.* 2001; 8(2): 322-324.

23. Alderman OLG, Lazareva L, Wilding MC, Benmore CJ, Heald SM, Johnson CE, et al. Local Structural Variation with Oxygen Fugacity in Fe_2SiO_{4+x} Fayalitic Iron Silicate Melts. *Geochim. Cosmochim. Ac.* 2017; 203: 15-36.
24. Farges F, Brown GE, Rehr JJ. Ti K-Edge XANES Studies of Ti Coordination and Disorder in Oxide Compounds: Comparison Between Theory and Experiment. *Phys. Rev. B.* 1997; 56(4): 1809.
25. Masuno A, Inoue H, Yu J, Arai Y. Refractive Index Dispersion, Optical Transmittance, and Raman Scattering of $BaTi_2O_5$ Glass. *J. Appl. Phys.* 2010; 108(6): 063520.
26. Alderman OLG, Ferlat G, Baroni A, Salanne M, Micoulaut M, Benmore CJ, et al. Liquid B_2O_3 up to 1700K: X-ray diffraction and boroxol ring dissolution. *J. Phys.: Condens. Matter.* 2015; 27(45): 455104.
27. Alderman OLG, Skinner LB, Benmore CJ, Tamalonis A, Weber JKR. Structure of Molten Titanium Dioxide. *Phys. Rev. B.* 2014; 90(9): 094204.
28. Alderman OLG, Benmore C, Neuefeind J, Tamalonis A, Weber R. Molten barium titanate: a high-pressure liquid silicate analogue. *J. Phys.: Condens. Matter.* 2019; 31(20): 20LT01.
29. Hannon AC. PFIT. http://www.alexhannon.co.uk/. Jan 18 2011.
30. Liu Q, Lange RA. The Partial Molar Volume and Thermal Expansivity of TiO_2 in Alkali Silicate Melts: Systematic Variation with Ti Coordination. *Geochim. Cosmochim. Ac.* 2001; 65(14): 2379-2393.
31. Dingwell DB. The Density of Titanium(IV) Oxide Liquid. *J. Am. Ceram. Soc.* 1991; 74(10): 2718-2719.
32. Yu J, Ishikawa T, Paradis P-F. Solidification and Thermophysical Property Studies of Barium Titanate Using Electrostatic Levitation Furnace. *J. Cryst. Growth.* 2006; 292(2): 480-484.
33. Ikemiya N, Yoshitomi J, Hara S, Ogino K. Surface Tensions and Densities of Melts in TiO_2-BaO and TiO_2-Na_2O Systems. *J. Jpn. I. Met.* 1993; 57(5): 527-532.
34. Seifert F, Paris E, Dingwell DB, Mottana A, Romano C, Davoli I. In Situ High Temperature Study of Titanium Coordination in a Rb-Silicate Glass and Liquid to 1400° C. *Glastechnische Berichte.* 1994: 221-227.
35. Mizutani N, Tajima Y, Kato M. Phase Relations in the System Y_2O_3-TiO_2. *J. Am. Ceram. Soc.* 1976; 59(3-4): 168-168.
36. Magunov R, Magunov I, Zagorodnyuk A. Sc_2O_3-TiO_2 System. *Ukr. Khim. Zh.* 2002; 68(9-10): 85-88.
37. Alderman OLG, Benmore CJ, Lin A, Tamalonis A, Weber JKR. Borate melt structure: Temperature dependent B-O bond lengths and coordination numbers from high-energy x-ray diffraction. *J. Am. Ceram. Soc.* 2018; 101(8): 3357-3371.
38. Alderman OLG. Borate melt structure: A short review. *Phys. Chem. Glasses: Eur. J. Glass Sci. Technol. B.* 2018; 59(1): 1-10.
39. Alderman OLG, Liska M, Machacek J, Benmore CJ, Lin A, Tamalonis A, et al. Temperature-driven structural transitions in molten sodium borates Na_2O-B_2O_3: X-ray diffraction, thermodynamic modelling and implications for topological constraint theory. *J. Phys. Chem. C.* 2016; 120(1): 553-560.
40. Skinner LB, Benmore CJ, Weber JKR, Du J, Neuefeind J, Tumber SK, et al. Low cation coordination in oxide melts. *Phys. Rev. Lett.* 2014; 112(15): 157801.
41. Yu J, Kohara S, Itoh K, Nozawa S, Miyoshi S, Arai Y, et al. Comprehensive Structural Study of Glassy and Metastable Crystalline $BaTi_2O_5$. *Chem. Mater.* 2009; 21(2): 259-263.
42. Schaller T, Stebbins JF. The Structural Role of Lanthanum and Yttrium in Aluminosilicate Glasses: A ^{27}Al and ^{17}O MAS NMR Study. *J. Phys. Chem. B.* 1998; 102(52): 10690-10697.
43. Yoshimaru K, Ueda Y, Morinaga K, Yanagase T. Glass Forming Region and Ti^{4+} Co-Ordination Number in R_2O−TiO_2 (R= Rb, K, Na) and BaO−TiO_2 Binary Glasses. *J. Ceram. Soc. Japan.* 1984; 92: 17-22.
44. Sakka S, Miyaji F, Fukumi K. Structure of Binary $K_2O.2TiO_2$ and Cs_2O-TiO_2 Glasses. *J. Non-Cryst. Solids.* 1989; 112(1-3): 64-68.

45. Sakka S, Miyaji F, Fukumi K. Study on the Structure of $K_2O.2TiO_2$ Glass by X-Ray Radial-Distribution Analysis. *J. Non-Cryst. Solids.* 1989; 107(2-3): 171-177.
46. Miyaji F, Yoko T, Kozuka H, Sakka S. Structure of $Na_2O{\cdot}2TiO_2$ Glass. *J. Mater. Sci.* 1991; 26(1): 248-252.
47. Duffy J, Ingram M. An interpretation of glass chemistry in terms of the optical basicity concept. *J. Non-Cryst. Solids.* 1976; 21(3): 373-410.
48. Greegor RB, Lytle FW, Sandstrom DR, Wong J, Schultz P. Investigation of TiO_2-SiO_2 Glasses by X-ray Absorption Spectroscopy. *J. Non-Cryst. Solids.* 1983; 55(1): 27-43.
49. Watanabe Y, Masuno A, Inoue H. Glass formation of rare earth aluminates by containerless processing. *J. Non-Cryst. Solids.* 2012; 358(24): 3563-3566.
50. Zhang M, Wen H, Yu H, Ai F, Shao H, Pan X, et al. Study on upconversion luminescence and thermal properties of Ho^{3+}/Yb^{3+} co-doped La_2O_3–TiO_2–ZrO_2 glasses. *J. Alloys Compd.* 2016; 672: 7-12.
51. Tangeman JA, Phillips BL, Navrotsky A, Weber J, Hixson AD, Key TS. Vitreous forsterite (Mg_2SiO_4): Synthesis, structure, and thermochemistry. *Geophys. Res. Lett.* 2001; 28(13): 2517-2520.
52. Menke Y, Baron V, Lemercier H, Hampshire S. Influence of the atmosphere on the oxidation state of the Eu-ion in a SiAlO(N) glass and glass-ceramic. pp. 277-282 in Mater. Sci. Forum. Vol. 325.
53. Brouder C, Cabaret D, Juhin A, Sainctavit P. Effect of atomic vibrations on the x-ray absorption spectra at the K edge of Al in α-Al_2O_3 and of Ti in TiO_2 rutile. *Phys. Rev. B.* 2010; 81(11): 115125.
54. Shannon RD. Revised Effective Ionic-Radii and Systematic Studies of Interatomic Distances in Halides and Chalcogenides. *Acta Crystallogr. A.* 1976; 32(Sep1): 751-767.
55. Škapin SD, Kolar D, Suvorov D. Phase stability and equilibria in the La_2O_3–TiO_2 system. *J. Eur. Ceram. Soc.* 2000; 20(8): 1179-1185.
56. Gong W, Zhang R. Phase relationship in the TiO_2–Nd_2O_3 pseudo-binary system. *J. Alloys Compd.* 2013; 548: 216-221.
57. Kolesnikov A, Sukhanova G, Zaitseva A, Shcherbakova L. High-temperature reaction of TiO_2 with Sm_2O_3. *Inorg. Mater. (Engl. Transl.).* 1987; 23(2): 222-224.
58. Waring J, Schneider S. Phase equilibrium relationships in the system Gd_2O_3-TiO_2. *Journal of Research at the National Bureau of Standards–A. Physics and Chemistry A.* 1965; 69: 255-261.
59. Shcherbakova L, Glushkova V, Guseva K, Mamsurova L, Sazonova L, Sukhanova G. Akad. Nauk SSSR, Neorg. Mat. 16, 1445-1449. *Inorg. Mater. (Engl. Transl.).* 1980; 16: 996-1000.
60. Shamrai G, Magunov R, Stasenko I, Zhirnova A. The Dy_2O_3-TiO_2 System. *Inorg. Mater.* 1989; 25(2): 233-235.
61. Shamrai G, Magunov R, Sadkovskaya L, Stasenko I, Kovalevskaya I. The System Ho_2O_3-TiO_2. *Inorg. Mater.* 1991; 27(1): 140-141.
62. Petrova M, Novikova A, Grebenshchikov R. Phase equilibria in the Er_2O_3-TiO_2 system. *Dokl. Akad. Nauk SSSR.* 1979; 246(1): 121-123.
63. Shamrai G, Magunov R, Stasenko I, Zhirnova A. The Tm_2O_3-TiO_2 System. *Russ. J. Inorg. Chem.+.* 1990; 35(3): 450-451.
64. Shamrai G, Zagorodnyuk A, Magunov R, Zhirnova A. Yb_2O_3-TiO_2 System. *Inorg. Mater.* 1992; 28(9): 1633-1635.
65. Shamrai G, Zagorodnyuk A, Magunov R. System Lu_2O_3-TiO_2. *Zh Neorg Khim+.* 1984; 29(12): 3168-3170.

Table 1: Properties of the rare earth ions and rare-earth sesquioxide-titanium dioxide systems. The ionic radii[54] are for trivalent cations in 6-fold coordination to oxygen, for sake of comparison. Hyphens (–) indicate lack of any glass formation for the $17RE_2O_3.83TiO_2$ compositions tested herein.

			Eutectic properties					Glass formation		
RE ion	***Z***	**Ionic radius (Å)**	**mol% RE_2O_3**	**mol% $REO_{1.5}$**	***T* (K)**	**Closest RE crystal phase mol% RE_2O_3**	**Ref.**	**mol% RE_2O_3**	**mol% $REO_{1.5}$**	**Ref.**
Sc	21	0.745	19	31.9	1746	50	[36]	–	–	This work
Y	39	0.9	∼10	∼18.2	1853	33.3	[35]	–	–	This work,[2]
La	57	1.032	17.3	29.5	1718	18.2	[55]	14-20	24.6-33.3	[1, 2, 3, 6]
Ce	58	1.01						11.1	20.0	[2] [b]
Pr	59	0.99						17.0	29.1	This work [a]
Nd	60	0.983	13.6	23.9	1716	18.2	[56]	15-20	26.1-33.3	[1, 3]
Pm	61	0.97								
Sm	62	0.958	10	18.2	1893	33.3	[57]	18.2	30.8	[5]
Eu	63	0.947						17.0	29.1	This work
Gd	64	0.938	∼14	∼24.6	1818	33.3	[58]	17.0	29.1	This work
Tb	65	0.923	13	23.0	1849	33.3	[59]	–	–	This work
Dy	66	0.912	17.5	29.8	1923	33.3	[60]			
Ho	67	0.901	20	33.3	1893	33.3	[61]	–	–	This work
Er	68	0.89	16	27.6	1973	33.3	[62]			
Tm	69	0.88	15	26.1	1873	33.3	[63]			
Yb	70	0.868	7	13.1	1893	33.3	[64]			
Lu	71	0.861	16.6	28.5	1793	33.3	[65]			

a. In argon gas flow only.

b. Batched as CeO_2.[2]

Table 2: Ti K-edge XANES measurement conditions and extracted pre-edge peak parameters for rare-earth titanates $17RE_2O_3.83TiO_2$. Pre-edge peak areas were obtained by integration from 4965 eV to 4972 eV, after subtraction of the main edge contribution, Fig. 2. The centroids are the first moments of the same distributions. The final column shows Ti–O coordination numbers predicted based on the linear relationship shown in Fig. 3c. Our analogous data for $BaTi_2O_5$[13] are also shown for reference.

RE or AE	**Gas**	***T* (K)**	**Phase**	**Centroid (eV) ± 0.10**	**Intensity (eV)**	n_{TiO}
Sc	O_2	2056(42)	Melt	4969.80	1.02(13)	5.05(20)
Sc	O_2	298	Solid	4970.18	0.40(5)	6.02(8)
Y	O_2	1993(34)	Melt	4969.74	1.10(15)	4.92(23)
Y	O_2	298	Solid	4970.33	0.37(5)	6.07(8)
Nd	O_2	1923(29)	Melt	4969.75	1.09(13)	4.94(20)
Nd	O_2	298	Glass	4969.90	0.73(9)	5.50(14)
Nd [a]	O_2	298	Glass	4969.99	0.67(7)	5.59(11)
La	O_2	1896(32)	Melt	4969.70	1.15(15)	4.84(24)
La	O_2	298	Glass	4969.90	0.76(10)	5.45(16)
La [a]	O_2	298	Glass	4969.99	0.65(6)	5.63(10)
La	Ar:5%CO	1926(37)	Melt	4969.74	1.19(16)	4.78(25)
La	Ar:5%CO	298	Solid	4969.97	0.41(5)	6.00(8)
Ba	O_2	1990(30)	Melt	4969.71	1.34(20)	4.55(31)
Ba	O_2	298	Glass	4969.84	0.98(15)	5.12(23)
Ba [a]	O_2	298	Glass	4969.84	0.93(9)	5.20(14)
Ba	Ar:5%CO	2032(32)	Melt	4969.69	1.36(20)	4.52(31)
Ba	Ar:5%CO	298	Solid	4970.25	0.69(10)	5.56(16)

a. Powder transmission measurement.

Table 3: High-energy x-ray diffraction measurement conditions and extracted peak parameters for lanthanum titanate $17La_2O_3.83TiO_2$. Glass density taken from Ref.,[6] melt density estimated as described in the main text. The first diffraction peak position Q_1 and full-width at half-maximum ΔQ_1 were obtained by Lorentzian peak fitting (including reflection through $Q = 0$). The final three columns list the distance, width and Ti–O coordination number for the first Ti–O correlation, Ti–O(1), as shown in Fig. 6. The first row values are taken from the literature,[6] for an 18.18 mol% La_2O_3 titanate glass. The second row corresponds to a Fourier transform with Q_{max} = 23.0 Å^{-1}, and the following rows to Q_{max} = 20.0 Å^{-1}.

T (K)	Phase	Mass density (g cm^{-3})	Number density (atoms Å^{-3})	Q_1 ± 0.10 (Å^{-1})	ΔQ_1 ± 0.14 (Å^{-1})	r_{TiO} (Å)	$\langle u^2_{TiO}\rangle^{0.5}$ (Å)	n_{TiO} ± 0.1
298	Glass[6]	4.89	0.0796	-	-	1.887	-	3.54
298	Glass	4.84	0.0801	2.09	0.53	1.906(2)	0.091(2)	4.5
298	Glass	4.84	0.0801	2.09	0.53	1.917(2)	0.102(2)	4.8
1456(27)	SCL	4.60	0.0760	2.02	0.76	1.870(3)	0.106(3)	4.1
1564(33)	SCL	4.56	0.0754	2.02	0.76	1.870(3)	0.106(3)	4.0
1659(36)	SCL	4.53	0.0749	2.01	0.79	1.870(3)	0.109(3)	4.0
1750(37)	Liquid	4.50	0.0745	2.01	0.81	1.866(3)	0.108(3)	3.9
1928(58)	Liquid	4.45	0.0735	2.01	0.82	1.868(4)	0.107(4)	3.8

Table 4: High-energy x-ray diffraction parameters for lanthanum titanate $17La_2O_3.83TiO_2$. Parameters for the liquids are approximate values obtained by taking the mean values for all five liquid temperatures. Columns 2 to 4 list the distance, width and Ti–O coordination number for the second Ti–O correlation, Ti–O(2), as shown in Fig. 6. A width parameter of zero means that the peak had instrumental broadening only, without any distribution of bond lengths. $\langle r_{TiO}\rangle$ and $\langle n_{TiO}\rangle$ are then the mean, or total values obtained for the asymmetric Ti–O correlation resulting from the sum of its two contributions. The final three columns give the mean O–Ti, O–La and O–M, where M = Ti,La, coordination numbers. The first row values are taken from the literature,[6] for an 18.18 mol% La_2O_3 titanate glass. The second row corresponds to a Fourier transform with Q_{max} = 23.0 Å^{-1}, and the following rows to Q_{max} = 20.0 Å^{-1}.

Phase	r_{TiO} (Å)	$\langle u^2_{TiO}\rangle^{0.5}$ (Å)	n_{TiO}	$\langle r_{TiO}\rangle$ (Å)	$\langle n_{TiO}\rangle$	r_{LaO} (Å)	$\langle u^2_{LaO}\rangle^{0.5}$ (Å)	n_{LaO}	$\langle n_{OTi}\rangle$	$\langle n_{OLa}\rangle$	$\langle n_{OM}\rangle$
Glass[6]	2.033	-	1.81	1.936	5.35	2.48	-	8.0	2.0	1.33	3.33
Glass	2.111(3)	0.001[a]	0.96(1)	1.942(2)	5.46(9)	2.531(4)	0.154(3)	9.4(2)	2.09(3)	1.47(3)	3.55(4)
Glass	2.123(9)	0.0(2)	0.45(8)	1.934(2)	5.28(11)	2.533(4)	0.157(5)	9.6(3)	2.02(4)	1.50(4)	3.53(6)
Liquids	2.15(1)	0.0(2)	0.7(3)	1.91(2)	4.7(2)	2.48(1)	0.21(2)	8.3(9)	1.79(9)	1.3(1)	3.09(7)

a. Fixed during fitting.

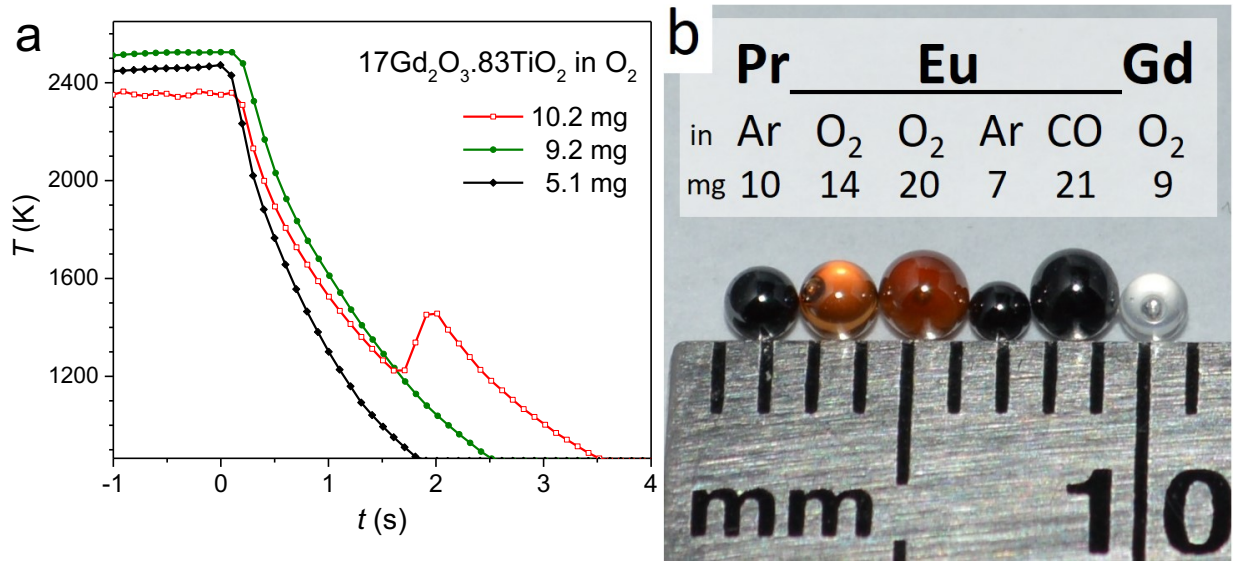

Figure 1: a) Temperature-time traces from 0.9 µm pyrometry, showing quenches of three different sized Gd titanate droplets. Time t = 0 corresponds to the heating laser being switched off. The largest droplet displays a recalescence event upon crystallization, while the smaller two vitrify to form glass beads. Note that temperatures can appear suppressed, and cooling rates enhanced, below ~1200 K due to partial transparency of the cooling glass at 0.9 µm.[16] b) Photograph of $17RE_2O_3.83TiO_2$ beads obtained by aerodynamic levitation in a nozzle open to the atmosphere, and quenching without displaying recalescence. RE element (Pr, Eu or Gd), levitation gas composition and bead masses in mg are all indicated, where CO denotes Ar:5%CO gas. The central two beads were observed to contain small crystalline fractions, whilst the other four were fully x-ray amorphous.

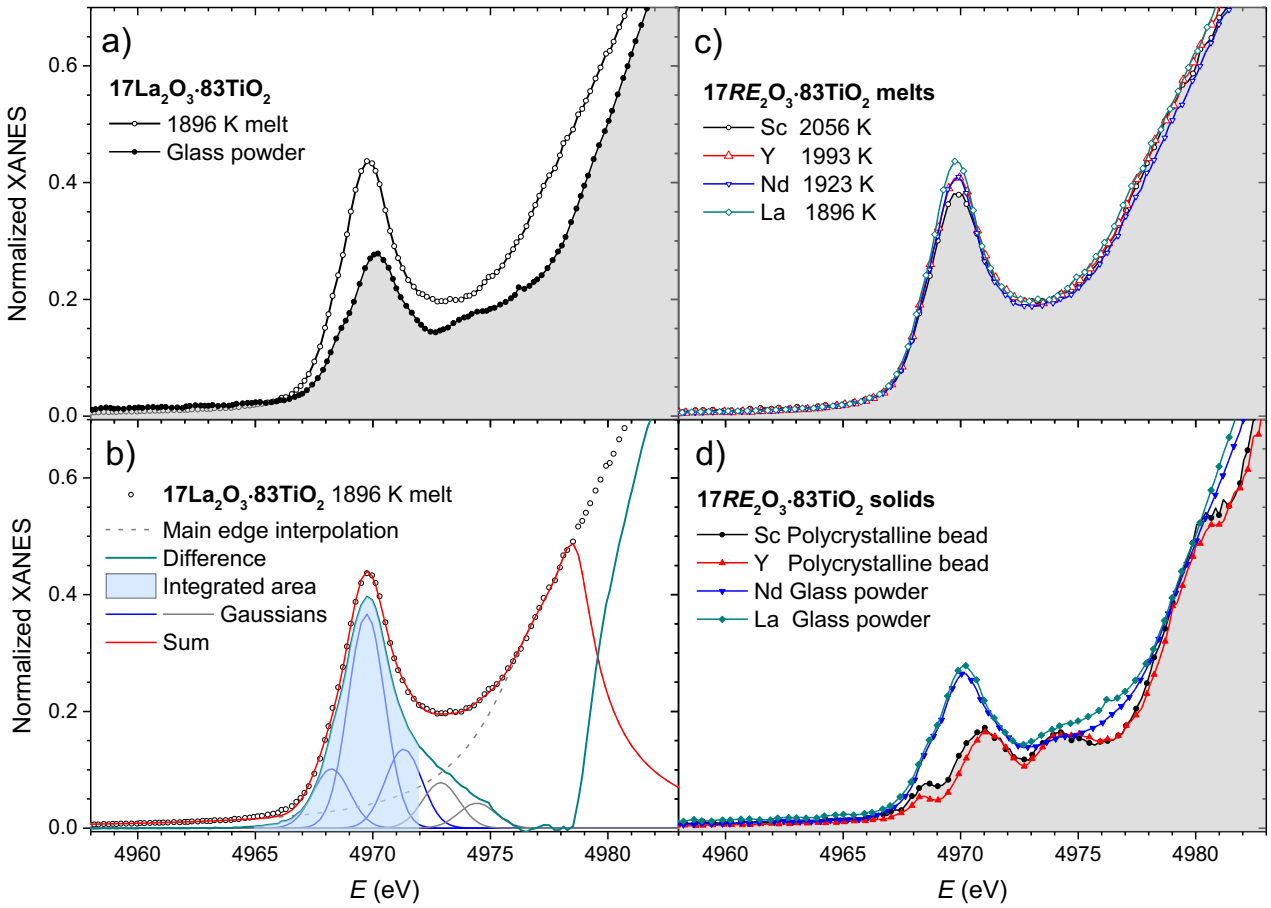

Figure 2: Pre-edge regions of Ti K-edge XANES spectra for molten and quenched rare-earth titanates $17RE_2O_3.83TiO_2$.

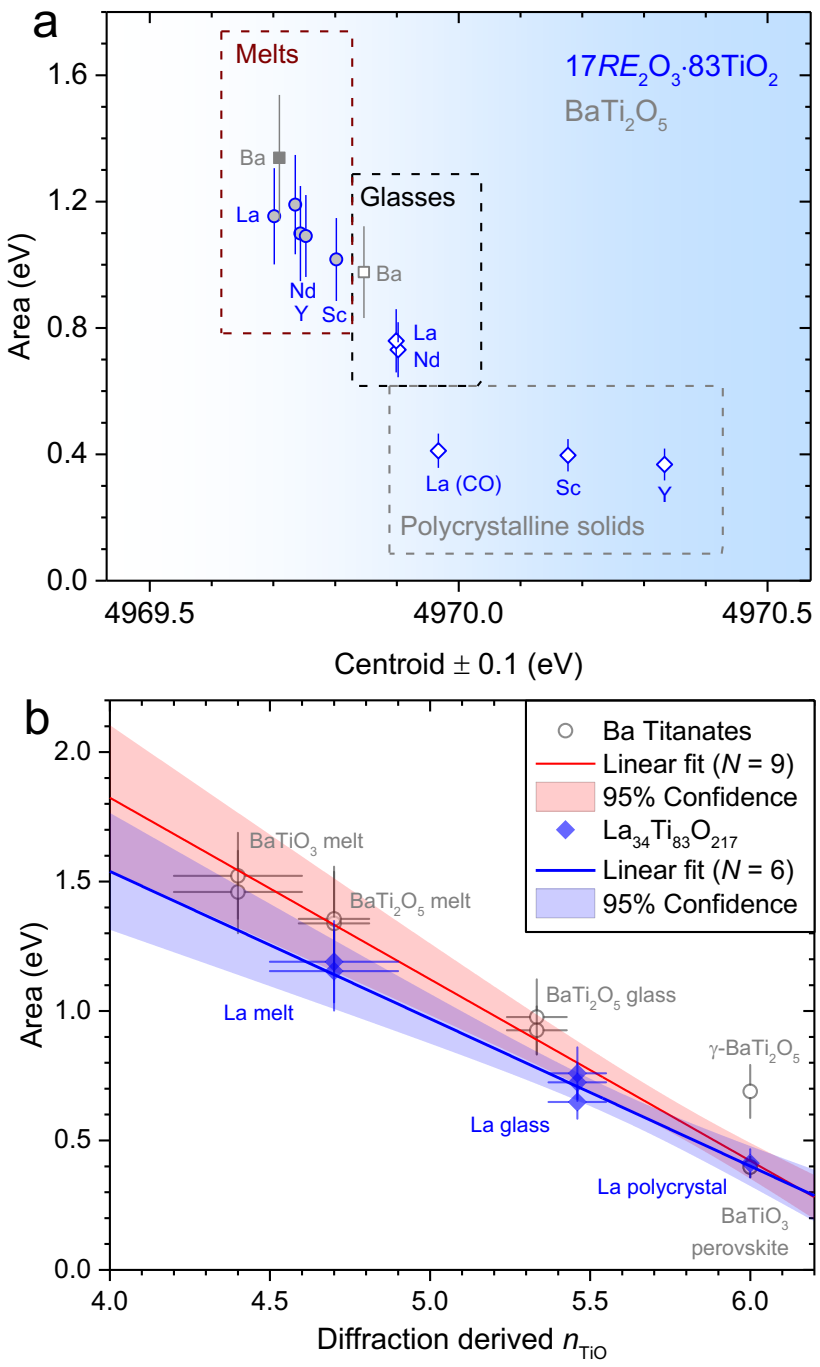
a
Melts
Glasses
Polycrystalline solids
17RE2O3·83TiO2
BaTi2O5
Ba
La
Nd
Y
Sc
Ba
La
Nd
La (CO)
Sc
Y
Area (eV)
Centroid ± 0.1 (eV)
b
Ba Titanates
Linear fit (N = 9)
95% Confidence
La34Ti83O217
Linear fit (N = 6)
95% Confidence
BaTiO3 melt
BaTi2O5 melt
La melt
BaTi2O5 glass
γ-BaTi2O5
La glass
La polycrystal
BaTiO3
perovskite
Area (eV)
Diffraction derived nTiO

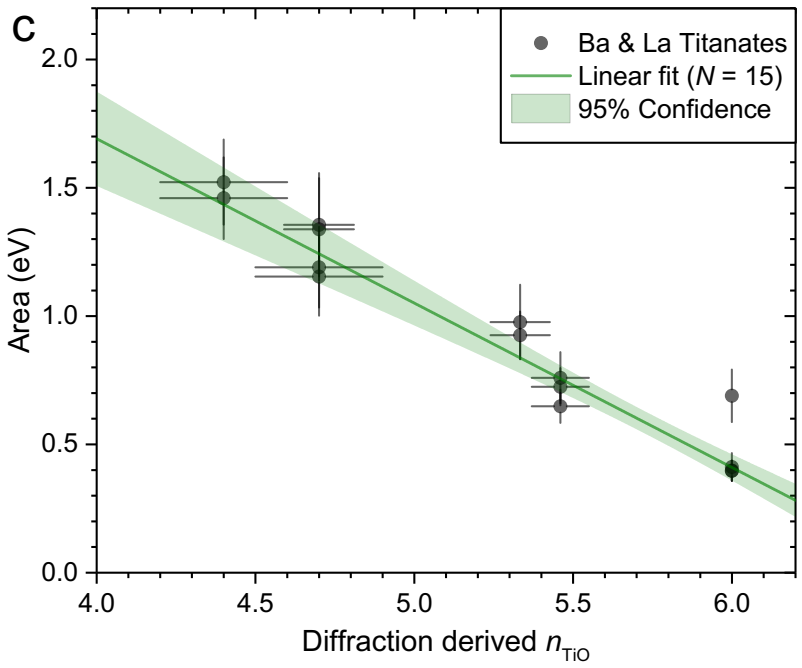

Figure 3: a) Summary of Ti K-edge pre-edge peak parameters for molten and quenched rare-earth titanates, compared to those for glass-forming $BaTi_2O_5$.[13] Pre-edge peak areas were obtained by integration from 4965 eV to 4972 eV, after subtraction of the main edge contribution. The centroids are the first moments of the same distribution. b) Pre-edge peak areas as a function of Ti–O coordination numbers, n_{TiO}, from diffraction measurements,[13, 28] with separate linear correlations shown for Ba and La titanates. c) As in part b, but with a linear fit to all N = 15 data points.

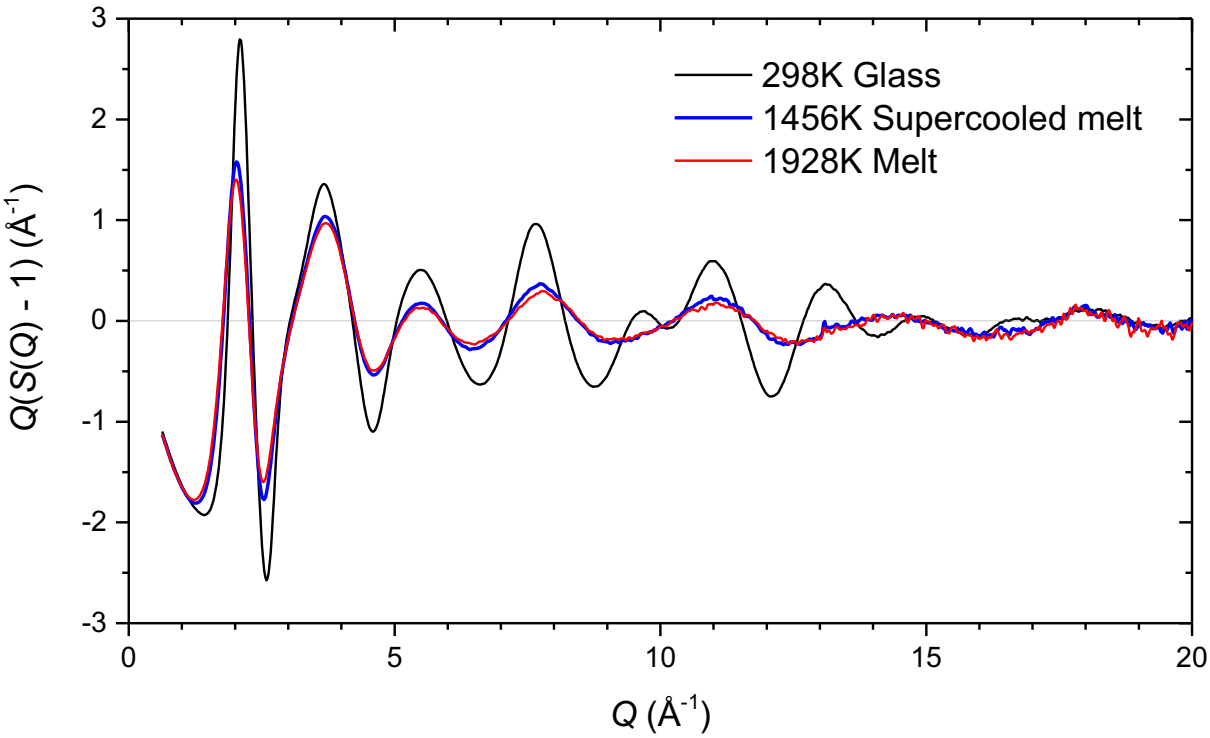

Figure 4: Interference functions, $Q(S(Q) - 1)$, for molten, supercooled liquid and glass of $17La_2O_3.83TiO_2$ composition. Only the results for the highest and lowest liquid temperatures are shown. The Q weighting of the structure factor, $S(Q) - 1$, helps to emphasize the high-Q features which correspond to the short-range structural ordering.

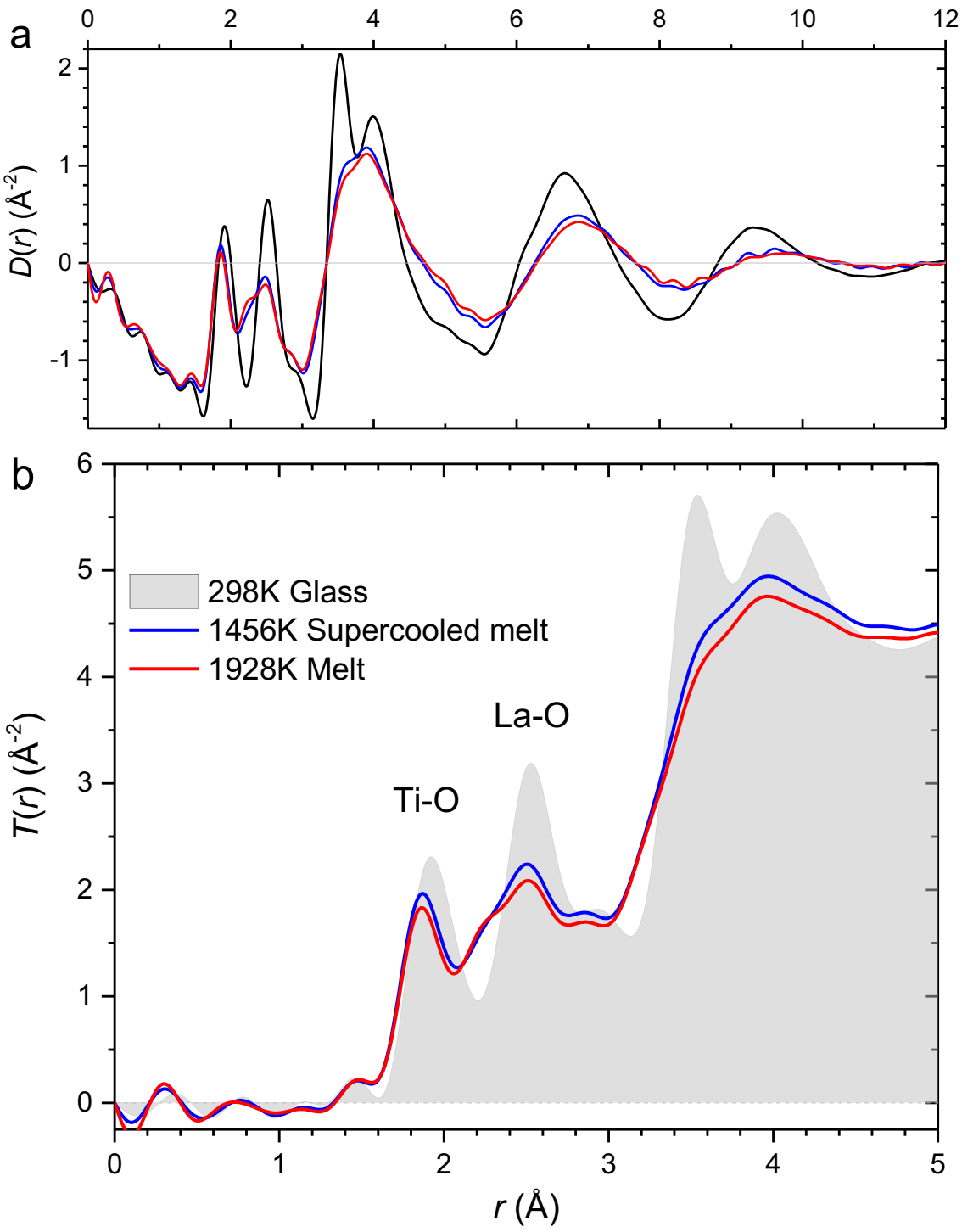

Figure 5: Correlation functions obtained by sine Fourier transform of the interference functions of Fig. 4, using a Q_{max} = 20.0 Å^{-1}. a) Differential distribution functions, $D(r)$, plotted out to 12 Å, showing the longer ranged features, dominated by cation-cation correlations. b) Total correlation functions, $T(r) = D(r) + 4\pi\rho_0 r$, showing the short-range structure.

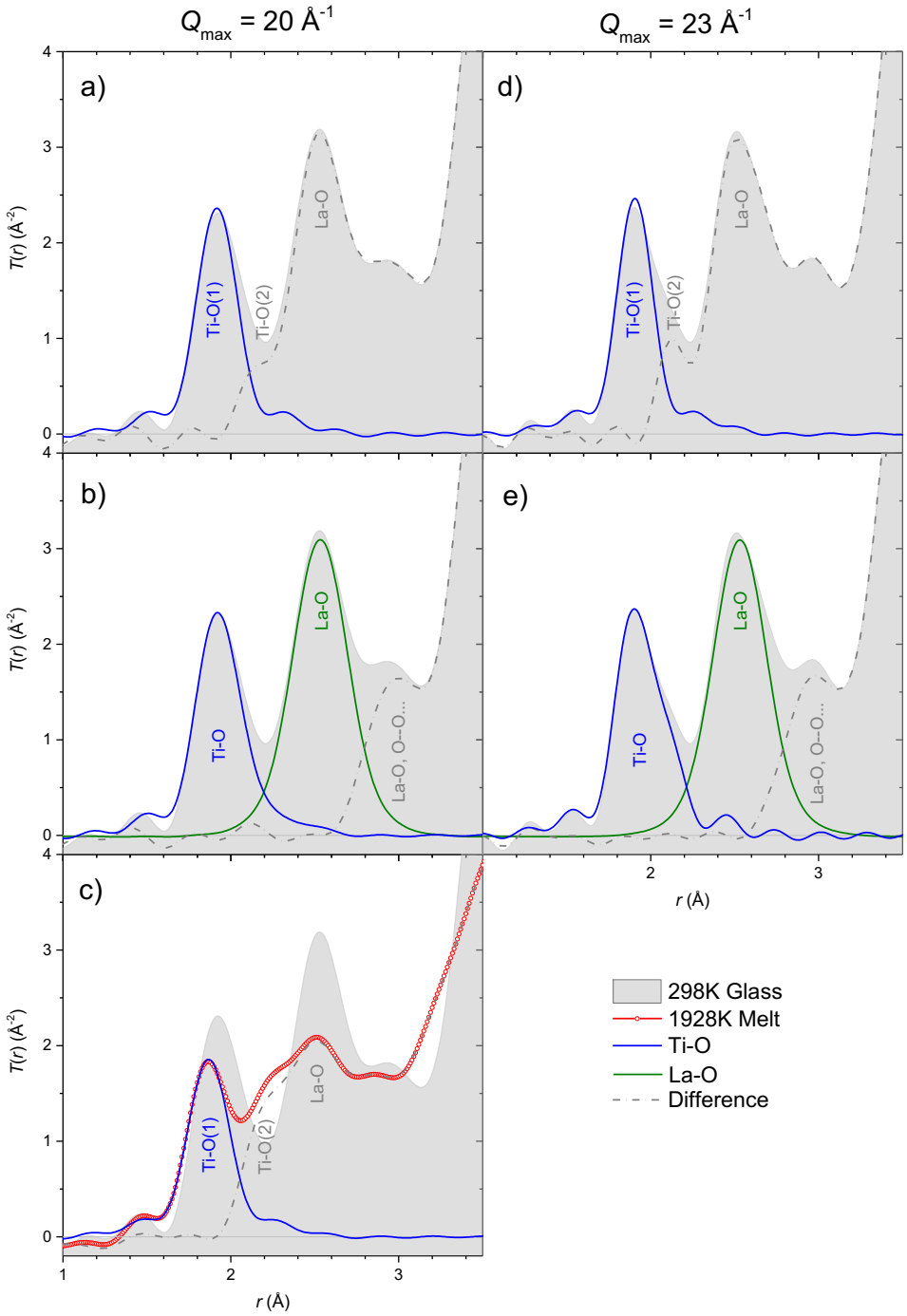

Figure 6: Peak fitting to $T(r)$ for liquid and glass of $17La_2O_3.83TiO_2$ composition. a) Leading-edge Ti-O peak fit, revealing a shoulder in the residual arising from longer Ti-O bonds. b) First Ti-O peak held fixed while a second contribution is fitted alongside the leading-edge of the La-O peak. The blue curve is the sum of the two Ti-O peaks. c) As in a), but for the liquid, and with the $T(r)$ for the glass still shown shaded for comparison. Parts a-c were Fourier transformed with a Q_{max} = 20.0 Å^{-1}, while parts d and e were derived from the glass $S(Q)$ up to Q_{max} = 23.0 Å^{-1}, yielding improved resolution. The latter was not feasible for the liquid due to the reduced counting statistics and increased thermal damping at high Q.

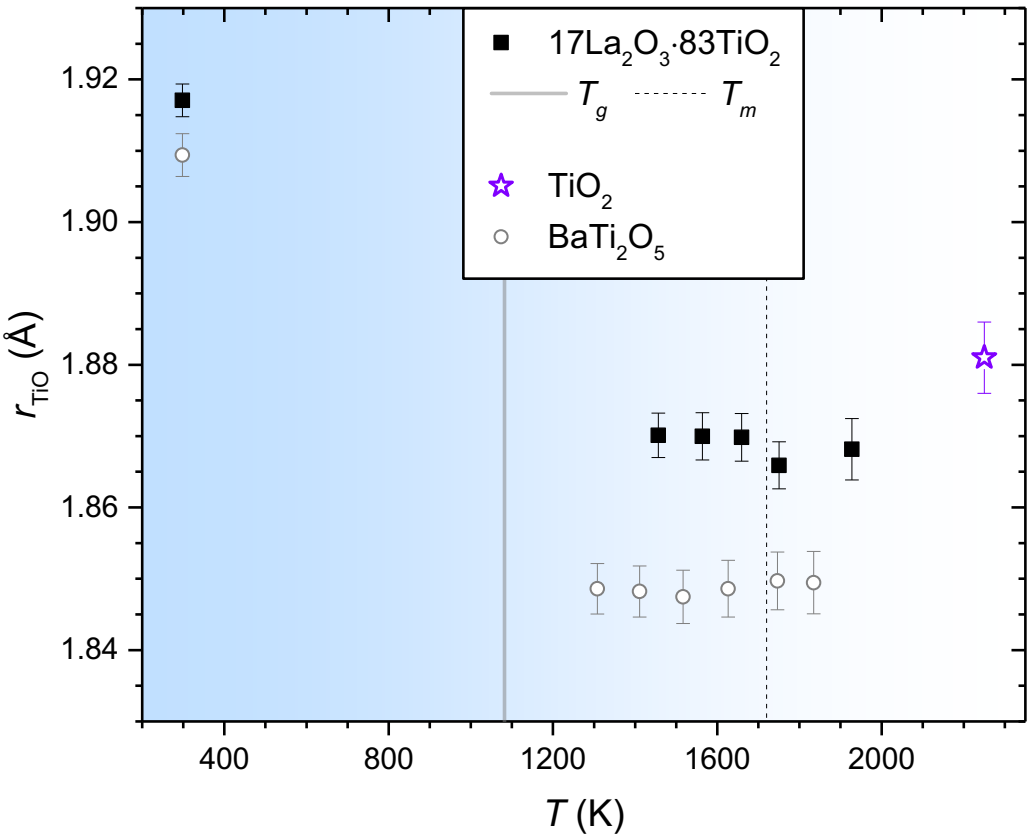

Figure 7: Position of the Ti–O peak obtained by fitting to its leading-edge in $T(r)$, as in Fig. 6a and 6c (Q_{max} = 20.0 Å^{-1}). Comparison is made between $17La_2O_3.83TiO_2$ and $BaTi_2O_5$[13] liquids and glasses, as well as molten TiO_2.[27] Vertical lines indicate T_g = 1082K and T_m = 1720K for the lanthanum titanate.

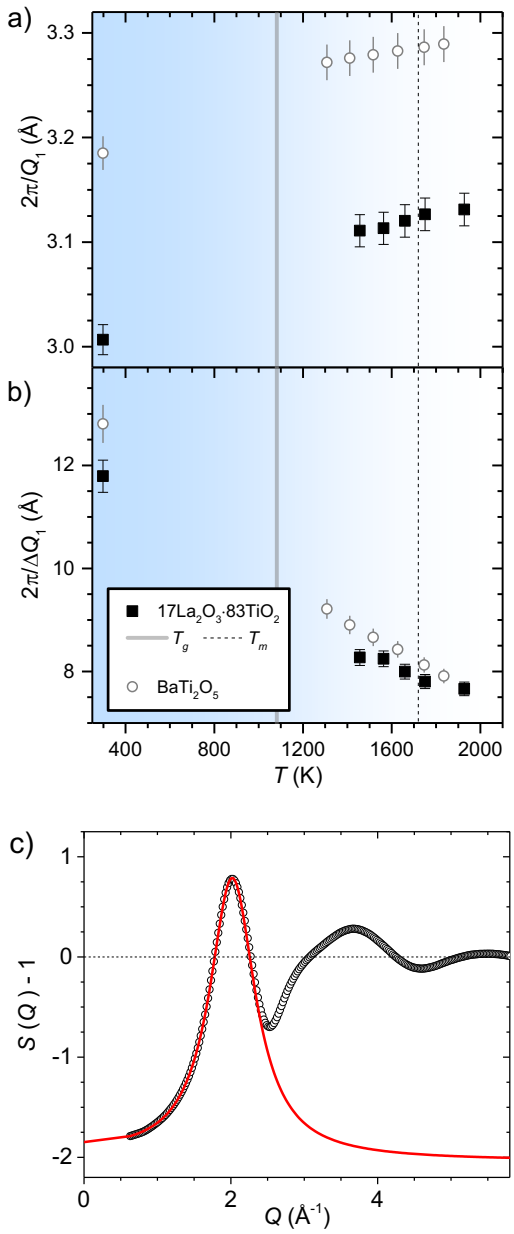

Figure 8: Parameters derived from Lorentzian fits to the first x-ray diffraction peak for $17La_2O_3.83TiO_2$ and $BaTi_2O_5$[13] liquids and glasses. a) Periodicities. b) Correlation lengths. c) Example fit (red solid line) for $17La_2O_3.83TiO_2$ supercooled liquid at 1456K.